Detailed investigation of the phase transition in $K_xP_4W_8O_{32}$ and experimental arguments for a charge density wave due to hidden nesting

Kamil Kolincio,[1,2] Olivier Pérez,[1] Sylvie Hébert,[1] Pierre Fertey,[3] and Alain Pautrat[1]

[1]*Laboratoire CRISMAT, UMR 6508 du CNRS et de l'Ensicaen, 6 boulevard Maréchal Juin, 14050 Caen, France*

[2]*Faculty of Applied Physics and Mathematics, Gdansk University of Technology, Narutowicza 11/12, 80-233 Gdansk, Poland*

[3]*Société civile Synchrotron SOLEIL, L'Orme des Merisiers, Saint-Aubin - BP 48, 91192 Gif-sur-Yvette, France*

(Received 24 February 2016; revised manuscript received 20 May 2016; published 15 June 2016)

Detailed structural and magnetotransport properties of monophosphate tungsten bronze $K_x(PO_2)_4(WO_3)_8$ single crystals are reported. Both galvanomagnetic and thermal properties are shown to be consistent with a charge density wave electronic transition due to hidden nesting of the quasi-1D portion of the Fermi surface. We also observe the enhancement of electronic anisotropy due to reconstruction of the Fermi surface at the Peierls transition. The resistivity presents a thermal hysteresis suggesting a first-order nature characteristic of a strong-coupling scenario. However, other measurements such as the change of carrier density demonstrate a second-order Peierls scenario with weak-coupling features. We suggest that the structural transition driven by the residual strain in the K-P-O environment is responsible for the resistivity hysteresis and modifies the Fermi surface which then helps the rise to the second-order Peierls instability.

DOI: 10.1103/PhysRevB.93.235126

I. INTRODUCTION

The low-dimensional oxides have always attracted wide attention due to their unconventional physics. The low-dimensional electronic structure leads to the anisotropy of transport and thermoelectric properties and/or to electronic instabilities, including modulation of electronic or spin structure, known as charge (or spin) density waves. Low dimensionality is also an important ingredient for superconducting transition in copper oxides, and the interplay of charge density waves (CDW) and superconductivity emerges as one of the central questions in that field [1]. $K_xP_4W_8O_{32}$ belongs to the monophosphate tungsten bronze (MPTB) family described by the general formula $A_x(PO_2)_4(WO_3)_{2m}$ (m being an integer, A = Na, K, Rb, Pb). The $(PO_2)_4(WO_3)_{2m}$ crystal structure is built by perovskite ReO_3-type infinite layers of corner-sharing WO_6 octahedra connected with PO_4 tetrahedra [2]. The regular family members possess quasipentagonal tunnels large enough to accommodate additional cations which results in change of their section to quasihexagonal [3]. Depending on the nature of the tunnels, monophosphate tungsten bronzes are classified as MPTBp and MPTBh. $K_xP_4W_8O_{32}$ belongs to MPTBp for $0 \leqslant x \leqslant 0.1$ and to MPTBh for $0.7 \leqslant x \leqslant 2$ [4]. It should be noted that the crystal structure of MPTB is similar to Mo_4O_{11} Magneli phases, built of MoO_6 octahedra perovskite-type layers isostructural to WO_6 and MoO_4 tetrahedra playing the same role in connecting Mo-O slabs as PO_4 in MPTB [5,6]. The MPTB low-m members exhibit 2D electronic character due to 5d conduction electrons concentrated in WO_6 layers [7]. The electrons are donated by PO_4 groups (each group donates one electron), which play the role of charge reservoir [8]. Since the quantity of the PO_4 groups is identical for each member, the number of conduction electrons per unit cell is independent of m and equal to 4 for undoped compounds. In $K_xP_4W_8O_{32}$ the conduction electron density is increased in comparison to its parent structure, $P_4W_8O_{32}$, due to the presence of K atoms, with the valence electron transferred to the conduction band. The number of electrons per unit cell is then $4 + x$. The undoped compounds exhibit anomalies in their resistivity associated with CDW transitions due to subsequent nesting of quasi-1D portions of the Fermi surface (FS). Such behavior has been explained in the framework of the hidden nesting scenario by Canadell and Whangbo [9]. For the low-MPTBp members, the electronic and structural transitions are observed at critical temperatures varying with m [2]. From x-ray and diffuse scattering, the modulation vectors associated with the structural distortions are found to be in general agreement with the calculated nesting vector, giving support to a Peierls scenario [5]. On the other hand, the genuine nature of transitions in MPTBh compounds is not clarified and remains one of the most interesting open questions in this family. Some of the physical properties of $K_xP_4W_8O_{32}$ were studied over a decade ago. Only a single anomaly has been observed in this compound [10], which is in contrast to the undoped $m = 4$, where two transitions were found [11]. This anomaly was observed for x varying from 0.86 to 1.94 with a maximum of $T^* = 170$ K for $x = 1.30$ [12]. The anomaly was also found in the thermoelectric power (TEP) at temperatures corresponding to values of T^* found for transition in resistivity curves. Moreover, the x-ray diffuse scattering experiments proved the existence of the long-range order, structural modulation with commensurate wave vector $q = (0.5; 0; 0)$ [12,13], unaffected by x. These results, together with the existence of a single electronic gap [14] revealed via the infrared reflectivity measurements, could be partially explained by a Peierls transition forecast by electronic structure calculations recalled above [9]. On the other hand, the fact that the q vector does not vary with x, thus with the band filling, was a source of controversy about the origin of the transition [12]. Furthermore, Bondarenko *et al.* [15] suggested that the relatively large anomaly observed in the specific heat at T^* is not consistent with a CDW transition but rather indicative of structural-only character of the transition. An alternative mechanism was proposed by Dusek *et al.* [13], explaining the transition as driven by the strain between potassium and the PO_4 tetrahedra causing displacement of the K, P, and O

 ©2016 American Physical Society

atoms. The nature of the transition observed in this material is then not clear. The scope of this work is to complement the information established beforehand with the new results and shed new light on the problem of presumed CDW existence in $K_xP_4W_8O_{32}$. In a broader perspective, this sample illustrates that a weak-coupling CDW can survive even if part of the lattice is significantly distorted.

II. EXPERIMENTAL

The single crystals with the typical size of 5 mm×1 mm×500 μm were grown using the chemical vapor transport method [16]. The potassium content was determined by EDS performed with SEM FEI XL 30 FEG. High-resolution x-ray diffuse scattering was studied on a selected high-quality single crystal with a size of 0.19×0.16×0.015 mm^3. Scans were executed using monochromated radiation with wavelength $\lambda = 0.50718$ Å and beam size of 200 μm×200 μm. The aim of the diffraction experiment being the measurement of a maximum of satellite reflections associated to the transition, data collection at low temperature (down to $T = 36$ K) was accomplished with the maximum flux of the beamline but also with an attenuator for limiting possible saturation of the CCD detector by the strong main reflections. The experiment was performed both at room temperature (RT) and at $T = 45$ K, thus far above and deep below the transition. The samples were cooled using a He gas blower. The electrical resistivity was measured using the four-probe method. The experiments were performed (when possible) in two directions: in the *ab* plane (ρ_{ab}) and out of plane (ρ_c). The contact configuration proposed by Hardy *et al.* [17], adapted for highly anisotropic systems [18,19], was used to measure ρ_c. The electrical contacts were made by welding 99.5% Al, 0.05% Si, 25 μm thick wires to the sample surface. The magnetoresistance was measured with electric current applied in the *ab* plane and magnetic field B maintained perpendicularly to the direction of electric field, in order to preserve a constant Lorenz force. The sample was rotated by θ, the angle between the B and c vectors. All magnetoresistance and resistivity measurements were performed using a physical properties measurement system (PPMS) from Quantum Design with a 14 T magnet and equipped with horizontal rotator. The thermopower was measured in the *ab* plane, with constant thermal gradient maintained between two chromel-constantan thermocouples soldered to the sample surface with indium. The thermocouples were also used to measure thermoelectric voltage, and the experiment was performed in the PPMS with external setup. The Hall coefficient was acquired by measuring transverse voltage between two points on the sample surface in the presence of longitudinal current and magnetic field applied perpendicularly to the *ab* plane. The magnetoresistance contribution was subtracted from the data. The dc magnetization was measured within a magnetic properties measurement system (SQUID-based MPMS from Quantum Design). The oriented single crystal was weighted and fixed with paper and scotch tape in a polyethylene straw. Constant magnetic field was applied along the *ab* plane. A high value of $B = 1$ T was used in order to achieve the finest scan resolution and extract the weak sample signal from substantially stronger background. The $I(V)$ curve was obtained by the four-probe method. The current was applied along the sample (in the *ab* plane) using a Keithley 228A source, and the voltage was measured with a microvoltmeter. The I contacts were enhanced by welding additional AlSi wires joined together with a small drop of DuPont 6838 silver paste. The sample was kept in liquid nitrogen to ensure effective contact cooling.

III. RESULTS AND DISCUSSION

A. Structural analysis

The purpose of the crystallographic study is to verify the results previously obtained by Dusek *et al.* [13]. In this previous study, the data were also achieved using synchrotron radiation, almost mandatory to solve the structure with such weak satellite peaks. 789 main and 409 satellite reflections with $I \geqslant 2.5\,\sigma(I)$ were then collected at 110 K, thus close to the transition temperature.

The reconstructed $(h0l)^*$ planes using the experimental frames collected with our single crystal at RT and 45 K (see Fig. 1) show unexpected extinction rules: rows running along c^* with a periodicity of ≈8.9 Å alternate with rows exhibiting a periodicity of ≈17.8 Å. This phenomenon can be interpreted using the hypothesis of the occurrence of twin domains related by a twofold axis parallel to c; our sample exhibits then a reticular pseudomerohedral twinning. The cell at RT was found to be monoclinic with the following cell parameters: $a = 6.676(1)$ Å, $b = 5.322(1)$ Å, $c = 8.899(1)$ Å, and $\beta = 100.637(2)^\circ$. The hypothesis of a reticular pseudomerohedral twinning has been successfully tested by a full structural refinement procedure for the RT data set.

The experiment performed at reduced temperature $T = 45$ K revealed the existence of weak superlattice reflections. In fact, two sets of additional peaks were found; they are corresponding to satellites associated with each twin domain as shown in Fig. 1 and they induce the doubling of the a parameter. The observation of these two sets is a supplementary proof validating our twin hypothesis. The positions of the satellites

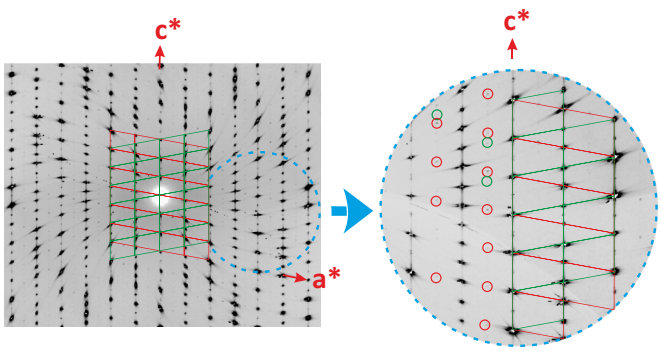

FIG. 1. $(h0l)^*$ plane at 45 K. Drawn green and red unit cells are related to the reticular pseudomerohedral twinning but refer to the RT cell, i.e., to $a \approx 6.68$ Å, $b \approx 5.32$ Å, $c \approx 8.90$ Å, and $\beta \approx 100.6^\circ$. In the zoom view, the satellite reflections leading to the doubling of the a parameter and associated with the transition are highlighted by red and green circles showing the satellites of red and green twin domains, respectively.

MOST WIEDZY Downloaded from mostwiedzy.pl

TABLE I. Positional coordinates and atomic displacement parameters.

Atom	Occupation	x	y	z	U_{eq} (Å^2)	$\|\Delta(\mathrm{RT}-45\ \mathrm{K})\|$ (Å)
W1a	1	−0.06936(3)	−0.25383(9)	0.58862(5)	0.00054(6)	0.021
W1b	1	−0.43044(3)	0.25641(10)	−0.58770(5)	0.00054(6)	0.034
W2a	1	−0.21793(4)	0.24434(9)	0.74920(5)	0.00052(6)	0.030
W2b	1	−0.28222(3)	−0.24711(8)	−0.74907(5)	0.00052(6)	0.016
Pb	1	0.3545(2)	0.2398(7)	0.1290(4)	0.0015(3)	0.054
Pa	1	−0.8546(2)	−0.2434(7)	−0.1298(4)	0.0015(3)	0.036
O1a	1	0.3664(6)	0.2387(19)	−0.0386(8)	0.0024(5)	0.066
O1b	1	−0.8691(6)	−0.2532(18)	0.0379(9)	0.0024(5)	0.022
O2a	1	0.3055(6)	−0.0143(15)	0.1582(10)	0.0025(5)	0.179
O2b	1	−0.8092(7)	−0.0002(15)	−0.1660(10)	0.0025(5)	0.155
O3a	1	−0.3225(6)	0.2358(16)	0.5760(9)	0.0033(6)	0.115
O3b	1	−0.1858(6)	−0.2418(16)	−0.5767(11)	0.0033(6)	0.049
O4a	1	0.4625(6)	0.266(2)	0.2222(9)	0.0030(5)	0.131
O4b	1	−0.9631(6)	−0.256(2)	−0.2218(10)	0.0030(5)	0.010
O5a	1	0.0112(6)	−0.0176(12)	0.4944(9)	0.0007(5)	0.190
O5b	1	−0.4997(5)	0.0081(12)	−0.5041(8)	0.0007(5)	0.057
O6a	1	−0.1439(6)	0.4945(14)	0.6855(9)	0.0015(5)	0.046
O6b	1	−0.3518(6)	−0.5164(14)	−0.6898(9)	0.0015(5)	0.145
O7a	1	−0.1364(7)	0.0030(15)	0.6903(10)	0.0016(5)	0.057
O7b	1	−0.3651(7)	−0.0200(15)	−0.6833(10)	0.0016(5)	0.129
O8a	1	0.2976(6)	0.4692(15)	0.1667(10)	0.0030(5)	0.104
O8b	1	−0.7880(6)	−0.4643(15)	−0.1587(9)	0.0030(5)	0.182
Ka	0.29(1)	−1.0697(7)	−0.2354(18)	−0.0011(10)	0.0042(10)	0.111
Kb	0.28(1)	0.5706(7)	0.246(2)	0.0027(11)	0.0042(10)	0.099

are in agreement both with the modulation vector previously reported by Dusek *et al.* [$q = (0.5; 0; 0)$] and with calculations performed by Canadell and Whangbo [9], who predicted this value as associated with hidden nesting of the 1D part of the Fermi surface. The diffraction pattern lead then to the following cell parameters: $a = 13.2383(6)$ Å, $b = 5.2823(1)$ Å, $c = 8.8511(2)$ Å, and $\beta = 100.677(3)$ Å.

The data recorded at 45 K at the Cristal beamline at Soleil contain 4113 observed reflections with $I \geqslant 3\,\sigma(I)$, 1703 reflections with $h = 2n + 1$ (i.e., satellites), and 2410 reflections with $h = 2n$ (i.e., main); indices refer to the unit cell above. The data set is then globally 3.4 times larger than the one collected by Dusek *et al.*, and we observe 4.15 times more satellite reflections directly related to the transition. Note that the data collection was performed deep below the transition temperature to achieve the largest possible enhancement of the satellite reflections. However, let us notice that our sample exhibits a reticular pseudomerohedral twinning; the two domains are related by a mirror perpendicular to a. The main reflections of both domains are fully or partly overlapped and the integration process requires additional corrections; the intensity of the main reflections is then expected to be less reliable than the fully separated satellites (see Fig. 1).

The refinement procedure was achieved using Jana2006 [20] in the 3-dimensional supercell with the space group $P2_1$ following the analysis of Dusek *et al.* The structure is fully described by 4 W, 2 P, 2 K, and 16 O atoms. The atomic displacement parameters (ADPs) were considered isotropic for O atoms and anisotropic in the other cases. Atoms related by inversion center in the centrosymmetric $P2_1/m$ approximation are restricted to have the same ADPs. The occupancy of the two K atoms is refined; they exhibit a partial occupancy of 0.291(4) and 0.279(4) leading to the chemical composition $K_{1.14(2)}P_4W_8O_{32}$, close to the expected formula. The final agreement factors, with 109 refined parameters, are 6.97% for the 4113 reflections, 6.78% for the 2410 reflections with $h = 2n$ and 8.05% for the 1703 reflections with $h = 2n + 1$. Atomic parameters of this refinement are given in Table I and atomic distances in Table II.

The structural results obtained at 45 K are compared with the analysis performed at room temperature (RT). The deviations between the atomic positions at 45 K and RT are reported in Table I. The maximum atomic displacements observed for the O, K, P, and W atoms are ≈ 0.19, 0.054, 0.111, and 0.034 Å, respectively (see Table I). These moderate values evidenced for W were already reported by Dusek *et al.* [13]; they did not induce any significant change in the W-W boundaries. Figure 3 shows the main modifications observed at 45 K for the cation-oxygen distances corresponding to the structure zones indicated in Fig. 2. The superstructure observed at 45 K does not induce the large distortions in the WO or PO bounding scheme [see mainly Figs. 3(b) and 3(c)]. The strongest effect is related to the geometry of the hexagonal windows [see Figs. 3(a) and 3(d)]. A dilatation of the cavities is observed in the direction of the Pa-Pa segment and a contraction in the perpendicular direction.

The paper written by Dusek *et al.* [13] provides a comparison between the average structure and the superstructure both calculated from the data collected at 110 K. Our present description details the differences observed between the structure of the fundamental state at room temperature and the structure at 45 K deep below the transition. The large number of

MOST WIEDZY Downloaded from mostwiedzy.pl

TABLE II. Interatomic distances. Symmetry codes: (i) $x,y,z+1$; (ii) $x+1,y,z+1$; (iii) $-x,y-1/2,-z+1$; (iv) $x,y-1,z$; (v) $x,y,z-1$; (vi) $x-1,y,z-1$; (vii) $-x-1,y+1/2,-z-1$; (viii) $x,y+1,z$; (ix) $-x-1,y+1/2,-z+1$; (x) $-x,y+1/2,-z+1$; (xi) $-x,y-1/2,-z-1$; (xii) $-x-1,y-1/2,-z-1$; (xiii) $x+1,y,z$; (xiv) $-x-1,y-1/2,-z$; (xv) $-x-1,y+1/2,-z$; (xvi) $-x,y-1/2,-z$; (xvii) $x,y-1,z-1$; (xviii) $-x+1,y-1/2,-z$; (xix) $-x+1,y+1/2,-z$; (xx) $-x,y+1/2,-z$; (xxi) $x+1,y+1,z+1$.

Boundary	d (Å)	Boundary	d (Å)	Boundary	d (Å)
W1a-O3b^{i}	1.920(8)	W1b-O3a^{v}	1.840(7)	W2a-O1b^{ix}	2.018(7)
W1a-O4b^{ii}	1.979(8)	W1b-O4a^{vi}	1.990(7)	W2a-O2a^{x}	1.999(9)
W1a-O5a	1.929(8)	W1b-O5b	1.833(7)	W2a-O3a	1.866(7)
W1a-O5a^{iii}	1.812(7)	W1b-O5b^{vii}	1.887(7)	W2a-O6a	1.797(8)
W1a-O6a^{iv}	1.947(8)	W1b-O6b^{viii}	1.921(8)	W2a-O7a	1.808(9)
W1a-O7a	1.932(9)	W1b-O7b	1.967(9)	W2a-O8a^{iii}	2.018(8)
W2b-O1a^{xi}	2.000(7)	Pa-O1b	1.532(9)	Pb-O1a	1.521(8)
W2b-O2b^{xii}	2.038(9)	Pa-O2b	1.478(9)	Pb-O2a	1.533(9)
W2b-O3b	1.799(8)	Pa-O4b	1.517(8)	Pb-O4a	1.520(8)
W2b-O6b	1.824(8)	Pa-O8b	1.513(9)	Pb-O8a	1.496(9)
W2b-O7b	1.794(9)				
W2b-O8b^{vii}	2.011(8)				
Ka-O1b^{xiii}	2.616(12)	Kb-O1a	2.660(12)		
Ka-O1b^{xiv}	2.854(13)	Kb-O1a^{xviii}	2.807(14)		
Ka-O1b^{xv}	2.675(13)	Kb-O1a^{xix}	2.734(14)		
Ka-O2a^{xvi}	3.499(12)	Kb-O2a^{xix}	2.681(14)		
Ka-O2b^{xiv}	2.755(13)	Kb-O2b^{xx}	3.489(12)		
Ka-O4b^{xiii}	2.615(14)	Kb-O4a	2.619(14)		
Ka-O4b^{xiv}	3.366(14)	Kb-O4a^{xviii}	3.201(14)		
Ka-O4b^{xv}	3.190(13)	Kb-O4a^{xix}	3.375(14)		
Ka-O6a^{xvii}	3.112(12)	Kb-O6b$^{?}$	3.000(12)		
Ka-O7a^{v}	2.989(12)	Kb-O7b^{ii}	3.089(12)		
Ka-O8a^{xvi}	3.284(12)	Kb-O8a^{xviii}	2.899(14)		
Ka-O8b^{xv}	2.931(13)	Kb-O8b^{xx}	3.154(12)		

observed independent satellite reflections (4.5 times more than in the previous study [13]) leads to a high degree of confidence in our result and very low standard deviations. This last point is very important since the differences observed above and below the transition are very weak in term of atomic positions (see Table I) and even slighter in term of distances (see Fig. 3). The obtained results clearly validate the conclusions drawn by Dusek *et al.* [13]: the main changes at 45 K occur for the phosphorus and potassium environment as shown by the variations of the K-O and P-O distances. However for us, such effect does not contradict the possibility of CDW formation since weak but significant deviations (≈0.01 to 0.02 Å) are also observed for W-W and W-O distances.

B. Physical properties

The typical in-plane resistivity vs temperature curves, measured for different x, are shown in Fig. 4. As previously reported [11,21], a clear anomaly is observed in the 100–150 K range at a temperature T^*, which depends on the potassium value. Additionally, a small thermal hysteresis is observed at the transition. To ensure that this effect is truly intrinsic to the sample and is not an artifact caused by insufficient thermalization, we have repeated the scan with heating/cooling

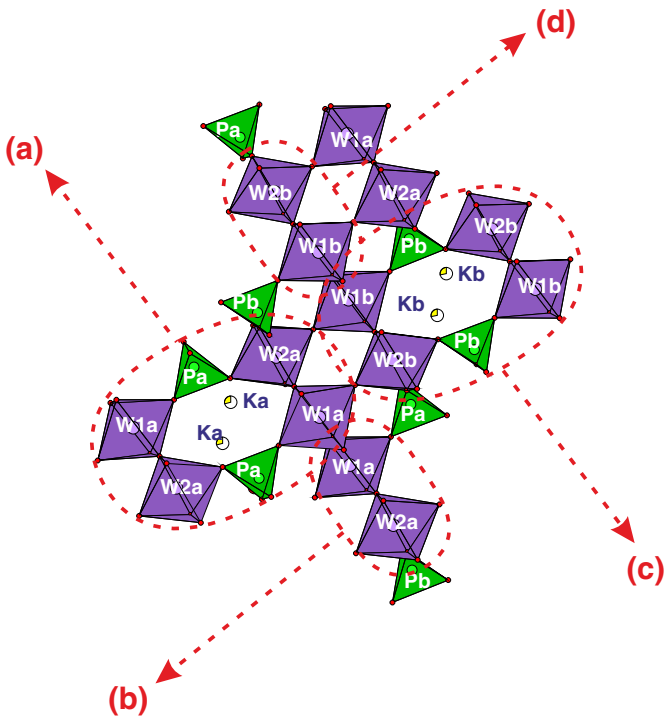

FIG. 2. Projection along **b** of an area of the structure exhibiting both the hexagonal tunnels and the $(WO_3)_m$ rows. WO_6 and PO_4 environments are drawn using purple and green colors, respectively. The (a), (b), (c), and (d) circled zones refer to Fig. 3.

rate as low as 0.05 K/min. As a result, we have found the reproducible hysteresis, with a very similar width of $\Delta T \approx 7$ K for $x = 1.21$ (shown in Fig. 5) and $x = 1.10$ and a smaller one ($\Delta T \approx 3$ K) for $x = 0.93$.

To go deeper insight into this anomaly, we have performed additional sample characterizations and analyzed in detail the distribution of potassium content in the crystals. The idea behind this is that any departure from a very precise stoichiometry could result in a broadening of the transition, as it is well known in high-T_c cuprates, for instance [22]. The performed EDS scans reveal that the sample's composition is not perfectly homogeneous at the sample scale. The K distribution for the $x = 1.10$ crystal is shown in Fig. 6. We find that it can be described by a Gaussian decay with $x = 1.10$ and FWHM $= 0.11$.

Considering the $T^*(x)$ dependence [21], one can expect a broadening of $\Delta T^* \approx 10$ K corresponding to the obtained distribution width. Note that, strictly, although ΔT^* stands in agreement with the hysteresis size only a broadening is expected by such a ΔT^* effect. One could consider the scenario of the current percolation in the preferential zones, which undergo the transition at various temperatures as an explanation of the macroscopic hysteresis; however this picture would lead to deviation from Ohmic behavior, which is not observed in our samples. Therefore, we find this mechanism irrelevant to explain the hysteretic manner of resistivity. Note that the existence of hysteresis can be a fingerprint of a first-order transition, *a priori* unexpected in the framework of Peierls-Frohlich theory which is a continuous second-order transition [23]. The Ginzburg-Landau approach predicts the

MOST WIEDZY Downloaded from mostwiedzy.pl

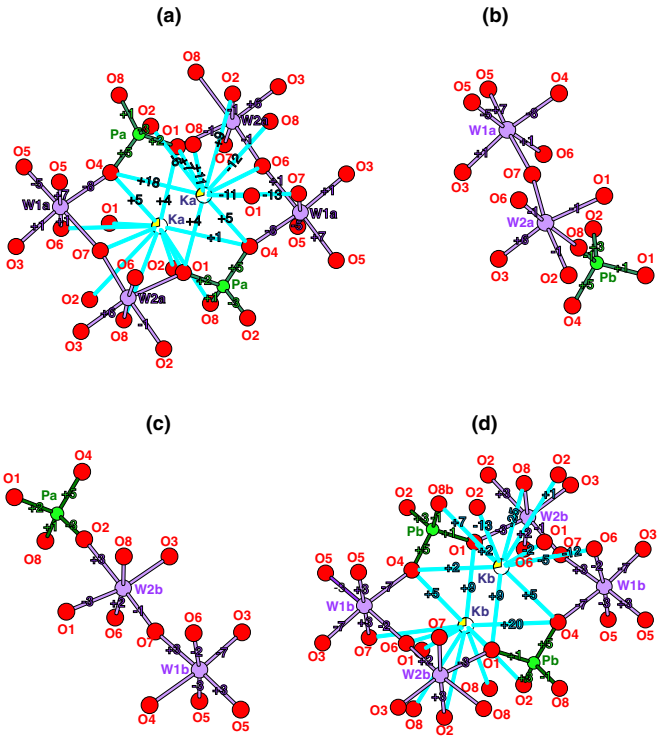

FIG. 3. Details of the projection drawn in Fig. 2. Numbers reported on the boundaries are related to the deviation observed between the room temperature and the 45 K structures for the corresponding distance; they are stated in hundredths of Å; a minus sign indicates a contraction at low temperature and a plus sign a dilatation.

first-order character of a lock-in transition separating an incommensurate state at high temperature and a commensurate state [24]. Such effects are observed in various CDW materials such as $TaSe_2$ [25] or $K_{0.3}MoO_3$ [26]. We find this case unlikely here, since neither transport nor structural properties reveal any sign of an incommensurate CDW at higher temperatures. However it should be noted that first-order transitions towards CDWs have been reported in $Lu_5Rh_4Si_{10}$ [27] and

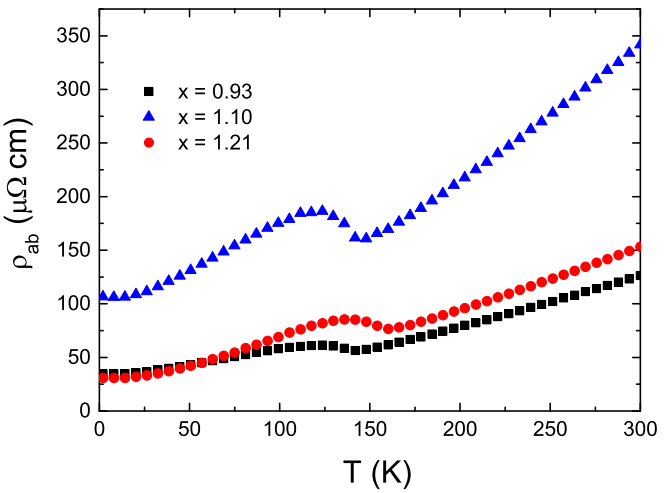

FIG. 4. In-plane resistivity vs temperature of $K_xP_4W_8O_{32}$ for various values of x.

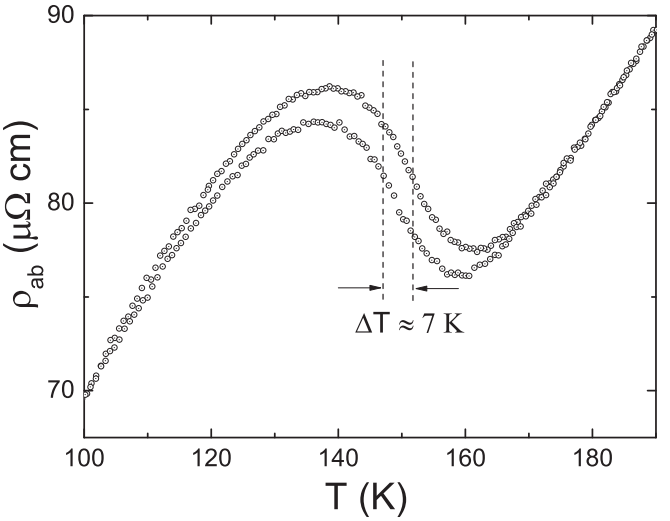

FIG. 5. Resistivity as a function of temperature around the suspected CDW transition in $K_{1.21}P_4W_8O_{32}$. The rate of temperature change during the heating and cooling procedure is 0.05 K/min.

$Lu_5Ir_4Si_{10}$ [28–30] without any signatures of the CDW phase at higher temperatures.

The anisotropy in electronic properties expected in a quasi-2D system is inferred by measurements of the out-of-plane resistivity ρ_c (Fig. 7). This latter shows a typical metallic behavior consistent with a coherent scattering perpendicular to the most conducting planes and an anomaly at T^*. The anisotropy of resistivity ρ_c/ρ_{ab} varies from 6 to 12 at room temperature. ρ_c/ρ_{ab} is strictly constant down to T^*, but remarkably grows from T^* to low temperature. This indicates a strong increase of the transport anisotropy. The reinforcement of anisotropy has been noted in materials with CDWs such as $NbSe_2$ [31], albeit without quantitative analysis. The constant electronic anisotropy for $T > T^*$ is consistent with a simple metallic state. For $T < T^*$, the strong change indicates that this anisotropy changes likely due to a Fermi surface reconstruction. It should also be noticed that the temperature variation of ρ_c/ρ_{ab} is very similar to the thermal dependence

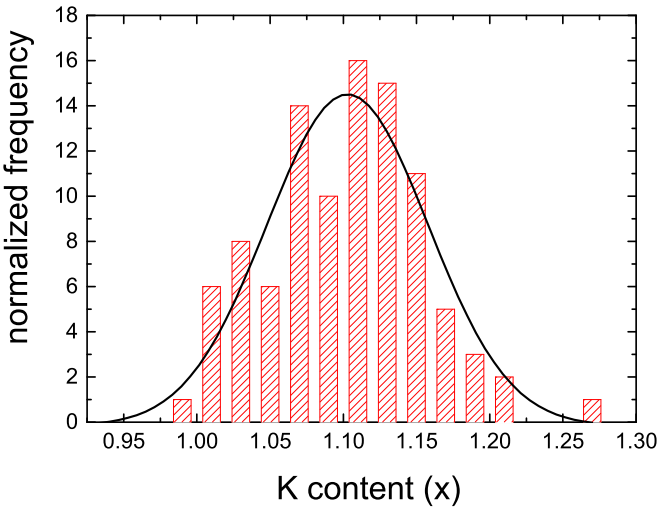

FIG. 6. Distribution of x with $K_xP_4W_8O_{32}$. Single crystal, and Gaussian decay fit (solid line).

MOST WIEDZY Downloaded from mostwiedzy.pl

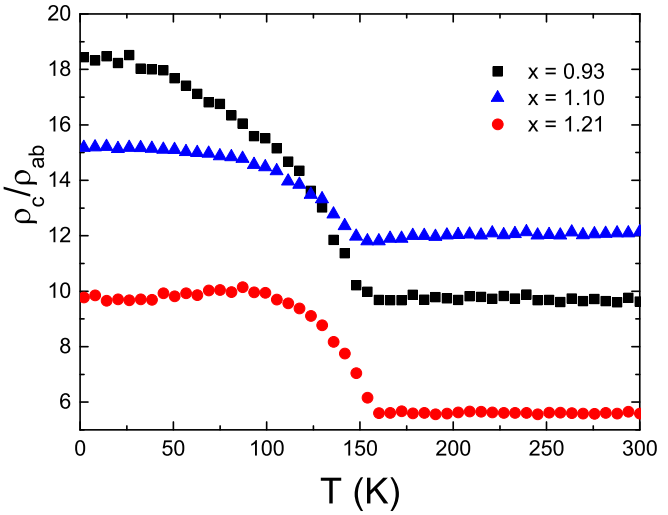

FIG. 7. Temperature dependence of ρ_c/ρ_{ab} ratio for various concentrations of potassium in $K_xP_4W_8O_{32}$.

of a Peierls gap. From this observation, at least, we can propose that its main origin is not from the change of electronic mobility of carriers, but rather from an anisotropic change of carrier density at T^*.

Magnetotransport measurements show a positive, metallic-like, magnetoresistance (MR), which increases significantly below T^*, as shown in Fig. 8. The MR follows a cosine law, reaching maximum for $B \perp c$, and is almost zero when B lies in the ab plane. The $\cos\theta$ regime followed by the magnetoresistance is a typical signature of the cylindrical, quasi-2D topology of the Fermi surface [32]. The MR can be discussed in the framework of Kohler's rule, predicting that all of Kohler's plots

$$\frac{\Delta\rho}{\rho_0} = F(\omega_c\tau) = F\left(\frac{H}{\rho(B=0,T)}\right) \quad (1)$$

(where ω_c is the cyclotron frequency and τ is the scattering time) follow the same curve, if τ is identical for all carriers, and constant in all parts of the Fermi surface [33]. In Fig. 9,

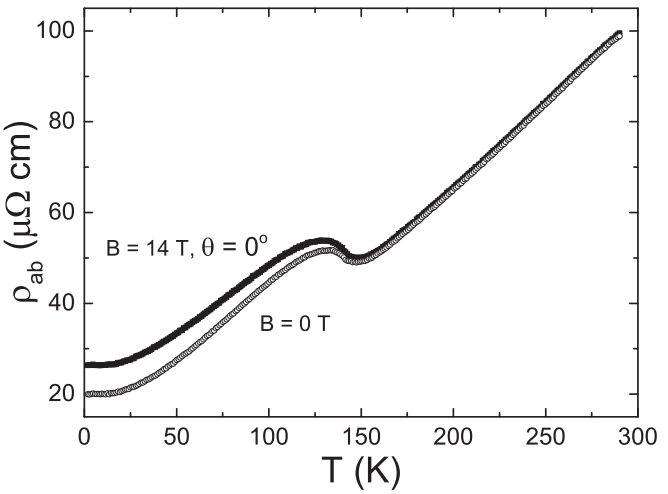

FIG. 8. Electrical resistivity and magnetoresistance in $K_{1.20}P_4W_8O_{32}$ as a function of temperature. θ is the angle between B and c^*.

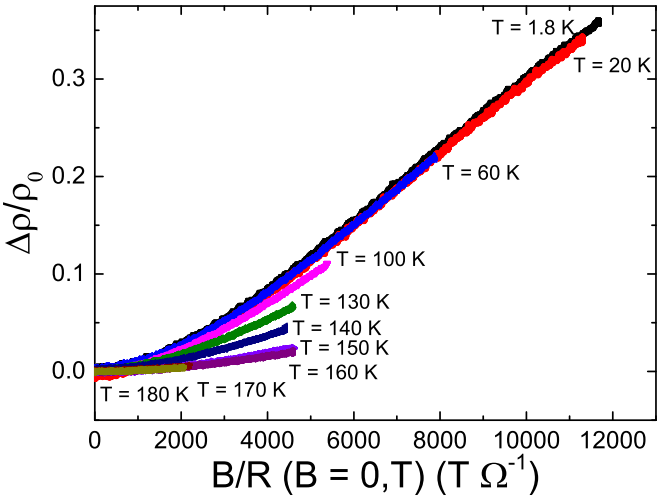

FIG. 9. Kohler's plot for $K_{1.20}P_4W_8O_{32}$.

we show the Kohler plot for the $x = 1.20$ sample. One can notice that all the curves for temperatures above $T^* \approx 158$ K fall into one line. When decreasing further the temperature, Kohlers's rule is violated down to $T \approx 60$ K, where it is again satisfied. Different causes can lead to a breakdown of Kohler's rule [33]. One possibility is the formation of a density wave at a critical temperature T_c and of a concomitant change of electronic structure, as observed in other materials with Peierls instability such as $NbSe_3$ [34]. In this case, the change is expected to be significant down to roughly $T_c/2$ where the gap starts to be fully open [23]. This is consistent with our observations.

The magnetic properties of a large oriented single crystal $K_{1.16}P_4W_8O_{32}$ with mass $m = 0.0744$ g have been measured. The background magnetization due to the sample holder was measured and carefully removed. Then the parasitic Curie-Weiss contribution (χ_C) due to paramagnetic impurities was quantified and subtracted from the data. The obtained magnetic susceptibility is shown in Fig. 10. Above T^*, χ is almost temperature independent, while for $T < T^*$ one observes a

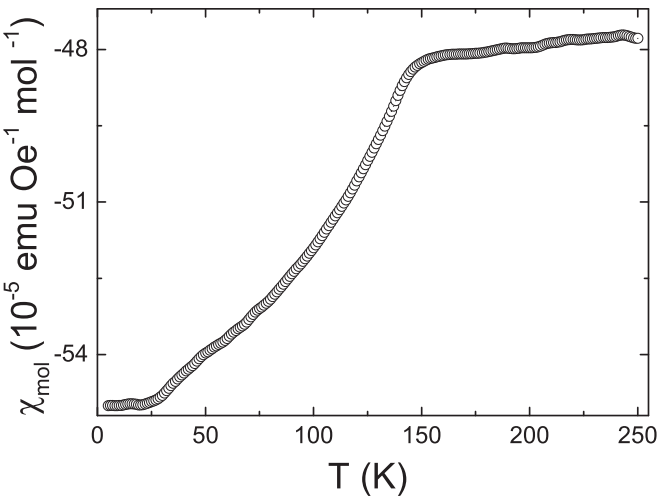

FIG. 10. Temperature dependence of the in-plane molar susceptibility of $K_{1.16}P_4W_8O_{32}$ corrected from background signal and the Curie-Weiss component.

MOST WIEDZY Downloaded from mostwiedzy.pl

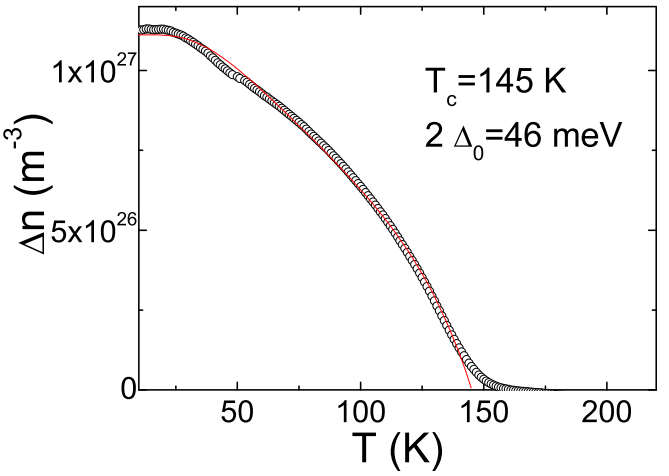

FIG. 11. Change of estimated carriers density as function of the temperature (dots). The solid line is a fit with a BCS-like expression (see text for details).

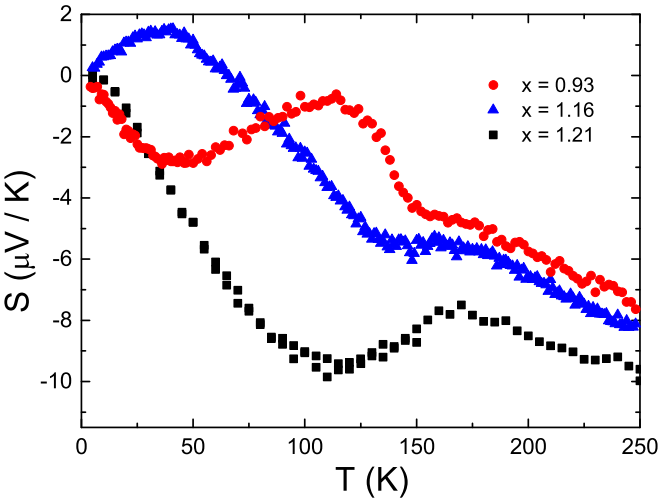

FIG. 12. Normalized thermopower as a function of temperature in $K_xP_4W_8O_{32}$ for different potassium concentrations.

notable drop of magnetic susceptibility, reminiscent of the decrease of χ due to the gap opening and CDW condensation of free electronic carriers reported in known CDW materials such as $Tl_{0.3}MoO_3$ [35], γ-Mo_4O_{11} [36], or in undoped MPTBp $m = 4$ [37].

To analyze the data, one has to consider the following contributions in a metallic-like sample:

$$\chi = \chi_{\text{ion}} + \chi_V + \chi_C + \chi_P + \chi_L. \tag{2}$$

The ion core diamagnetism, χ_{ion}, and the Van Vleck paramagnetism of ions, χ_V, were assumed to be constant with temperature. From the remaining ingredients—χ_P, the Pauli paramagnetism of conduction electrons, and the Landau diamagnetism of carriers, χ_L—we have deduced the number of condensed electrons as a function of temperature, shown in Fig. 11. The maximum $\Delta n \approx 1.12\times10^{27}$ m^{-3} corresponds to 15% of the electronic density calculated from chemical formula ($n_0 = 8.16\times10^{27}$ m^{-3}).

In a BCS-Peierls description of the CDW transition, the number of condensed electrons follows the temperature variation [38]

$$n_{\text{condensed}} = n_0 \frac{\Delta(T)}{\Delta_0} \tanh\left(\frac{\Delta(T)}{2k_BT}\right) \tag{3}$$

with the electronic gap

$$\Delta(T) = \Delta_0 \tanh\left[\frac{\pi k_B T_C}{\Delta_0}\sqrt{1.018\left(\frac{T_C}{T}-1\right)}\right], \tag{4}$$

where Δ_0 is the electronic gap at $T = 0$ K. Here, we find a good fit with a BCS mean-field weak-coupling expression. A slightly better fit can be proposed when removing the low-temperature part ($T < 40$ K) where the raw data are affected by the parasitic Curie-Weiss contribution. However, since this does not change significantly the fitting parameters, we prefer to show the fit on all the $T < 150$ K part. We have found the electronic gap $2\Delta_0 = 46$ meV for $x = 1.15$, which converges with the value predicted by mean-field model in the limit of weak electron-phonon coupling $2\Delta = 3.52\,kT^* \approx 44.6$ meV. Here, we have to mention the work of Haffner *et al.* [14] who have measured the infrared absorption of $K_{1.30}P_4W_8O_{32}$. They report at low-temperature absorption peaks which were tentatively attributed to single-particle excitations across a gap. In this framework, a value $2\Delta \approx 43$ meV can be deduced. It is worth noting that this value compares extremely well with our magnetization data and this indicates that condensed carriers are effectively at the origin of these absorption peaks as proposed by Haffner *et al.*

To gain deeper insight into the change of carrier density upon the transition, we have conducted the study of thermopower with various potassium concentrations. The temperature dependence of the Seebeck coefficient for different values of x is shown in Fig. 12. All $S(T)$ present a transition between two metallic regimes, with linear $S(T)$ curves, at low and high temperatures. In the transition region, depending on x, the transition is associated with an increase of S ($x = 0.93$), a decrease of S ($x = 1.21$), or for the intermediate doping ($x = 1.16$), a constant value of S. The thermopower even turns positive at low temperature for $x = 1.16$. The above described behaviors are in good agreement with the results reported previously [10,21]. The maximum in $S(T)$ close to $S = 0$ indicates enhancement of the hole influence for $x = 0.93$. On the other hand, electrons remain dominant carriers in the $x = 1.21$ compound. Roussel *et al.* [10] suggested that strong change of slope and existence of an extremum, either in the positive or negative direction, might result from Peierls transition with high-mobility carriers left in the pockets remaining after imperfect nesting of the Fermi surface. To follow the thermal evolution of the effective electronic density n_{eff} containing both the electron and hole contributions (with opposite signs), we have applied the semiclassical 3D model of quasifree electrons [39]:

$$S_{3D} = -\left(\frac{3}{2}+\lambda\right)\left(\frac{\pi}{3}\right)^{\frac{2}{3}} \frac{k_B^2 m_e T}{e\hbar^2 n_{\text{eff}}^{\frac{2}{3}}}. \tag{5}$$

The carrier density at high temperature (n_{HT}) and the loss of carriers due to the transition (Δn_{eff}) were estimated from the linear parts of $S(T)$ at high and low temperatures, respectively, with an assumption that the in-plane effective mass $m^* = m_e$

MOST WIEDZY Downloaded from mostwiedzy.pl

TABLE III. Effective carrier concentrations in $K_xP_4W_8O_{32}$ for different doping, estimated from $S(T)$ with semiclassical 3D model.

K content	n_{chem} (10^{27} m^{-3})	n_{HT} (10^{27} m^{-3})	$\frac{\Delta n_{eff}}{n_{HT}}$ (%)
0.93	7.88	2.72	22.20
1.10	8.16	2.26	12.13
1.16	8.28	2.35	34.16
1.21	8.34	4.70	8.67

and is constant with T both for electrons and holes. We have assumed the scattering factor $\lambda = -\frac{1}{2}$, corresponding to scattering with acoustic phonons. The obtained n_{HT} (effective electronic density) for $T > T^*$ is for each sample (see Table III) reasonably close to the values calculated from the chemical formula (n_{chem}). For $x = 1.16$, one can compare the concentration of condensed carriers deduced from both the magnetic measurements and the Seebeck measurements. We find respectively $\Delta n = 1.12\times10^{27}$ m^{-3} and $\Delta n_{eff} = 2.35\times10^{27}$ m^{-3}, which are in rather good agreement. This shows that the used model, despite its roughness, can serve as a useful guide in the estimation of carrier density in quasi-2D metals.

The Δn_{eff} found in compounds with visible hole contribution are notably higher than the one found for $x = 1.21$, where the electrons are dominant in the whole temperature range. This effect can be explained as caused both by condensation of electrons, thus their removal from the conduction band, and the increase of the role of light holes, which contribute to n_{eff} with sign opposite to electrons.

The investigation of the existence of CDWs in low-dimensional materials must not omit the search for non-Ohmic dc transport. The evidence of Fröhlich transport has already been reported in a number of quasi-1D materials such as $NbSe_3$ [40], $K_{0.3}MoO_3$ [41,42], and $Tl_{0.3}MoO_3$ [35], while the attempts to observe CDW sliding in quasi-2D materials were unsuccessful even in powerful electric fields [43] with the exception of only a single compound, $DyTe_3$ [44]. The difficulty with the study of this effect arises both from notably stronger pinning observed in 2D systems and from metallicity which remains in 2D materials after imperfect nesting of the Fermi surface, which obstructs reaching strong electric fields. We have performed the measurement of the $I(V)$ curve in the $K_{1.15}P_4W_8O_{32}$ sample cooled in liquid nitrogen applying dc current up to $I = 6$ A, reaching a maximum electric field of $E = 121$ mV/cm. No break of linearity in dc transport was found in this temperature range. We also emphasize that while the CDW nesting vector doubles the cell periodicity, the depinning energy can be significantly increased by the commensurability term [45–47] which can even prevail over the impurity pinning as in quasi-1D $(2,5(OCH_3)_2DCNQI)_2Li$ [48]. Note that the maximum E we have reached is a factor of 5 smaller than the minimum threshold field in $DyTe_3$ which rises further at temperatures far below T^* and the commensurability term in $K_xP_4W_8O_{32}$ is expected to raise the pinning potential to the values comparable to the electronic gap. We suggest that the lack of observed nonlinearity is caused by strong pinning arising both from the commensurate nature of the modulation and from the 2D electronic character of the tested material. Therefore, the lack of nonlinearity in dc transport cannot contradict the CDW scenario in $K_xP_4W_8O_{32}$.

C. Discussion

The nature of the transitions observed in $K_xP_4W_8O_{32}$ was the subject of an intensive dispute. Drouard *et al.* [12] remarked that the modulation vector should significantly vary with x, while for each x one observes the identical $q = 0.50a^*$ modulation vector. On the contrary, the band structure calculations performed by Canadell *et al.* [9] predict that the modulation vector associated with hidden nesting of the quasi-1D part of the $K_xP_4W_8O_{32}$ Fermi surface varies from $0.47a^*$ to $0.50a^*$ for $x = 0.8$ and $x = 3.5$, respectively, and this deviation is far from significant. Bondarenko *et al.* [15] concluded that the large (in comparison to the undoped $m = 4$) change in the specific heat due to transition observed at T^* indicates that the transition is essentially structural and not a simple CDW transition. Nevertheless, we find the comparison between $\Delta C_p/Rp$ (p is the number of electrons per formula unit and $R = 8.31$ J mol^{-1} K^{-1} is the gas constant) in $K_xP_4W_8O_{32}$ and corresponding quantities in "well established" CDW materials misguiding. Considering both electrons donated by P groups and K atoms in the tunnels, the value of p should be 5.07, 5.30, and 5.45 for $x = 1.07$, $x = 1.30$, and $x = 1.45$, respectively, instead of values slightly larger than unity considered by Bondarenko *et al.* Then, we find that $\Delta C_p/Rp$ for $K_xP_4W_8O_{32}$ should vary between 0.27 and 0.47 for $x = 1.07$ and $x = 1.45$, respectively, which is finally smaller than the values found in examples of known CDW materials $K_{0.3}MoO_3$ (0.53), KMo_6O_{17} (0.40), or η-Mo_4O_{11} (0.78), recalled by Bondarenko *et al.* Then, the argument that $\Delta C_p/Rp$ is too large to be attributed to a single CDW transition appears not very strong. Dusek *et al.* [13] suggested that the transition is driven by atomic displacements due to strain induced between K atoms and the PO_4 tetrahedra instead of the CDW formation. We agree that this mechanism would produce a change in the electronic band structure, but its effect is not essential to explain the physical properties showing modification of the Fermi surface accompanied with carrier condensation. The small hysteresis observed in resistivity is indicative of a first-order transition, suggesting the strong lattice component of the observed anomaly. Such scenario is expected in a strong-coupling approach [49]. On the other hand, this model predicts the electronic gap to be substantially larger than the weak-coupling value of $2\Delta = 3.52\,kT^*$ [50,51]. This is not relevant in $K_xP_4W_8O_{32}$, since our results show the excellent agreement between the measured electronic gap and the weak-coupling prediction. In the strong-coupling scenario, at $T > T^*$, the short order fluctuations are still preserved leading to diffuse scattering in the vicinity of superlattice reflections observed below T^* [52] which is not visible in our sample even with synchrotron radiation. Another interesting point is also the weakness of structural distortion in the W-O assembly–displacements in W-O and W-W distances are 0.01 to 0.02 Å 0.01 to 0.02 Å. Ludecke *et al.* [53] shown that the largest atomic displacements due the structural modulation accompanying CDW in MPTB [2,54] correspond to the W atoms. Then, in search for the clues for the character of the transition, one shall consider only the changes in the W-O bonding scheme and the low values found by us do not corroborate with the requirement of

MOST WIEDZY Downloaded from mostwiedzy.pl

large distortions in strong-coupling mode. The BCS character of condensed electronic density and electronic gap are strong arguments for a genuine second-order nature of the electronic part of the transition. Note that the hysteresis is not visible in magnetic susceptibility. Then, it is reasonable to assume that the hysteretic behavior of resistivity likely originates from the structural distortion in the K-P-O environment which produces an additional effect on the scattering term. In this picture, if one considers the residual strain between K atoms and PO_4 tetrahedra as a main driving force of the structural transition in $K_xP_4W_8O_{32}$, the Peierls instability can be seen as a by-product of the structure modification. The evolution of a band structure upon the transition allows the nesting of a 1D fragment of the Fermi surface with a preferential wave vector $q = 0.5a^*$, independently of x, and overcomes the suppression of the CDW [55] due to the disorder caused by inhomogeneous potassium distribution. Then, it is favorable to maintain this commensurate value unchanged with K content to preserve the optimal nesting conditions. This sort of resonance of CDW and the underlying lattice leading to the existence of one privileged modulation vector can partially explain the lack of subsequent nesting of remaining Fermi surface parts as predicted by Canadell and Whangbo [9] or observed in undoped $P_4W_8O_{32}$ [11].

IV. CONCLUSIONS

In this article, we report a full set of experimental data on $K_xP_4W_8O_{32}$, including new high-resolution x-ray data, magnetic susceptibility, and detailed chemical characterization to focus on the nature of the transition observed at T^*. We conclude that the anomalies observed in physical properties of $K_x(PO_2)_4(WO_3)_8$ are associated with condensation of around 15% of the total number of carriers and the hidden nesting of the quasi-1D portion of the Fermi surface. We also find the enhancement of transport property anisotropy upon the FS modification. Despite the resistivity hysteresis, we have provided strong evidence for the weak-coupling Peierls scenario. We propose that the thermal hysteresis does not arise from first-order characteristics, but from scattering due to residual strains around the structural transition, which also modifies the Fermi surface and enables the second-order charge density wave instability.

ACKNOWLEDGMENTS

Financial support by the French National Research Agency ODACE ANR, Grant No. ANR-11-BS04-0004, is gratefully acknowledged.

[1] M. Leroux, M. Le Tacon, M. Calandra, L. Cario, M.-A. Méasson, P. Diener, E. Borrissenko, A. Bosak, and P. Rodière, Phys. Rev. B **86**, 155125 (2012).
[2] P. L. P. Roussel and O. Pérez, Acta Crystallogr., Sect. B: Struct. Sci. **57**, 603 (2001).
[3] B. Domenges, M. Hervieu, B. Raveau, and M. O'Keeffe, J. Solid State Chem. **72**, 155 (1988).
[4] P. Roussel, D. Groult, A. Maignan, and P. Labbé, Chem. Mater. **11**, 2049 (1999).
[5] P. Foury-Leylekian and J.-P. Pouget, Solid State Sci. **4**, 387 (2002).
[6] E. Canadell, M. H. Whangbo, C. Schlenker, and C. Escribe-Filippini, Inorg. Chem. **28**, 1466 (1989).
[7] B. Domenges, N. McGuire, and M. O'Keeffe, J. Solid State Chem. **56**, 94 (1985).
[8] P. Roussel, P. Labbé, H. Leligny, D. Groult, P. Foury-Leylekian, and J. P. Pouget, Phys. Rev. B **62**, 176 (2000).
[9] E. Canadell and M.-H. Whangbo, Phys. Rev. B **43**, 1894 (1991).
[10] P. Roussel, D. Groult, C. Hess, P. Labbe, and C. Schlenker, J. Phys.: Condens. Matter **9**, 7081 (1997).
[11] J. Dumas, U. Beierlein, S. Drouard, and C. Schlenker, Solid State Sci. **4**, 379 (2002).
[12] S. Drouard, P. Foury, P. Roussel, D. Groult, J. Dumas, J. Pouget, and C. Schlenker, Synth. Met. **103**, 2636 (1999).
[13] M. Dusek, J. Ludecke, and S. van Smaalen, J. Mater. Chem. **12**, 1408 (2002).
[14] S. Haffner, M. Dressel, D. Groult, and C. Schlenker, Eur. Phys. J. B **24**, 167 (2001).
[15] V. Bondarenko, J. Brill, J. Dumas, and C. Schlenker, Solid State Commun. **129**, 211 (2004).
[16] J. Giroult, M. Goreaud, P. Labbe, and B. Raveau, J. Solid State Chem. **44**, 407 (1982).
[17] V. Hardy, A. Maignan, C. Martin, F. Warmont, and J. Provost, Phys. Rev. B **56**, 130 (1997).
[18] F. Warmont, V. Hardy, J. Provost, D. Grebille, and C. Simon, Phys. Rev. B **57**, 7485 (1998).
[19] G. Villard, A. Daignere, A. Maignan, and A. Ruyter, J. Appl. Phys. **84**, 5080 (1998).
[20] V. Petříček, M. Dušek, and L. Palatinus, Z. Kristallogr. - Cryst. Mater. **229**, 345 (2014).
[21] S. Drouard, D. Groult, J. Dumas, R. Buder, and C. Schlenker, Eur. Phys. J. B **16**, 593 (2000).
[22] D. Shi, M. S. Boley, M. Patel, R. K. Kalia, and P. Vashishta, J. Appl. Phys. **66**, 2074 (1989).
[23] G. Grüner, Rev. Mod. Phys. **60**, 1129 (1988).
[24] W. L. McMillan, Phys. Rev. B **12**, 1187 (1975).
[25] D. E. Moncton, J. D. Axe, and F. J. DiSalvo, Phys. Rev. B **16**, 801 (1977).
[26] R. M. Fleming, L. F. Schneemeyer, and D. E. Moncton, Phys. Rev. B **31**, 899 (1985).
[27] C. S. Lue, Y.-K. Kuo, F. H. Hsu, H. H. Li, H. D. Yang, P. S. Fodor, and L. E. Wenger, Phys. Rev. B **66**, 033101 (2002).
[28] B. Becker, N. G. Patil, S. Ramakrishnan, A. A. Menovsky, G. J. Nieuwenhuys, J. A. Mydosh, M. Kohgi, and K. Iwasa, Phys. Rev. B **59**, 7266 (1999).
[29] M. Leroux, P. Rodière, and C. Opagiste, J. Supercond. Novel Magn. **26**, 1669 (2012).
[30] M. H. Jung, H. C. Kim, A. Migliori, F. Galli, and J. A. Mydosh, Phys. Rev. B **68**, 132102 (2003).
[31] A. LeBlanc and A. Nader, Solid State Commun. **150**, 1346 (2010).

MOST WIEDZY Downloaded from mostwiedzy.pl

[32] A. Pippard, *Magnetoresistance in Metals*, Cambridge Studies in Low Temperature Physics (Cambridge University Press, Cambridge, UK, 1989).
[33] R. H. McKenzie, J. S. Qualls, S. Y. Han, and J. S. Brooks, Phys. Rev. B **57**, 11854 (1998).
[34] S. Yasuzuka, K. Yamaya, Y. Okajima, S. Tanda, N. Takeshita, H. Mitamura, T. Nakanishi, and N. Môri, J. Phys. Soc. Jpn. **74**, 1787 (2005).
[35] B. Collins, K. Ramanujachary, M. Greenblatt, and J. Waszczak, Solid State Commun. **56**, 1023 (1985).
[36] C. Schlenker, S. Parkin, and H. Guyot, J. Magn. Magn. Mater. **54–57**, Part 3, 1313 (1986).
[37] Z. S. Teweldemedhin, K. V. Ramanujachary, and M. Greenblatt, Phys. Rev. B **46**, 7897 (1992).
[38] R. Khasanov, P. W. Klamut, A. Shengelaya, Z. Bukowski, I. M. Savić, C. Baines, and H. Keller, Phys. Rev. B **78**, 014502 (2008).
[39] I. Pallecchi, M. Codda, E. Galleani d'Agliano, D. Marré, A. D. Caviglia, N. Reyren, S. Gariglio, and J.-M. Triscone, Phys. Rev. B **81**, 085414 (2010).
[40] P. Monceau, N. P. Ong, A. M. Portis, A. Meerschaut, and J. Rouxel, Phys. Rev. Lett. **37**, 602 (1976).
[41] J. Dumas, C. Schlenker, J. Marcus, and R. Buder, Phys. Rev. Lett. **50**, 757 (1983).
[42] L. Forró, J. R. Cooper, A. Jánossy, and K. Kamarás, Phys. Rev. B **34**, 9047 (1986).
[43] F. DiSalvo and R. Fleming, Solid State Commun. **35**, 685 (1980).
[44] A. A. Sinchenko, P. Lejay, and P. Monceau, Phys. Rev. B **85**, 241104 (2012).
[45] P. A. Lee and T. M. Rice, Phys. Rev. B **19**, 3970 (1979).
[46] P. Lee, T. Rice, and P. Anderson, Solid State Commun. **14**, 703 (1974).
[47] J. Dumas and D. Feinberg, Europhys. Lett. **2**, 555 (1986).
[48] S. Tomić, N. Biškup, M. Pinterić, J. U. von Schütz, H. Schmitt, and R. Moret, Europhys. Lett. **38**, 219 (1997).
[49] W. L. McMillan, Phys. Rev. B **16**, 643 (1977).
[50] R. S. Kwok, G. Gruner, and S. E. Brown, Phys. Rev. Lett. **65**, 365 (1990).
[51] A. Smontara, K. Biljakovic, J. Mazuer, P. Monceau, and F. Levy, J. Phys.: Condens. Matter **4**, 3273 (1992).
[52] K. Rossnagel, J. Phys.: Condens. Matter **23**, 213001 (2011).
[53] J. Ludecke, A. Jobst, and S. van Smaalen, Europhys. Lett. **49**, 357 (2000).
[54] P. Foury-Leylekian, E. Sandré, S. Ravy, J.-P. Pouget, E. Elkaim, P. Roussel, D. Groult, and P. Labbé, Phys. Rev. B **66**, 075116 (2002).
[55] J. P. Pouget and R. Comes, in *Charge Density Waves in Solids*, edited by L. P. Gor'kov and G. Grüner, Modern Problems in Condensed Matter Sciences (Elsevier, Amsterdam, 1989), Vol. 25, pp. 85–136.

MOST WIEDZY Downloaded from mostwiedzy.pl